# Evaporation of Sessile Drops on Polymer Surfaces: Ellipsoidal Cap Geometry

**H. Yildirim Erbil***

*TUBITAK, Marmara Research Center, Department of Chemistry, P.O. Box 21, 41470, Gebze, Kocaeli, Turkey*

**R. Alsan Meric**†

*Istanbul Technical University, Faculty of Aeronautics and Astronautics, Maslak, Istanbul 80626, Turkey*

*Received: January 24, 1997; In Final Form: April 9, 1997*⊗

The evaporation rate of sessile drops of water resting on poly(methyl methacrylate) polymer has been studied by using the recently published precise data of Rowan, Newton, and McHale. Mathematical expressions for an ellipsoidal cap drop resting on a solid surface having three parameters (base radius, height, and contact angle) are first derived. A vapor diffusion model of a drop based on a simplified two-parameter ellipsoidal cap geometry is also developed similar to Rowan et al. The expression for the rate of evaporation in the latter model reduces to that of Rowan et al.'s two-parameter model in the limit, as the drop shape becomes a spherical cap geometry. It is seen that the drop heights as calculated from the two-parameter ellipsoidal cap model fit the experimental data better than those evaluated from the spherical cap model. When the three-parameter ellipsoidal cap model is used, the surface area and volume of the drop show almost complete linear time dependence for most of the data.

## Introduction

The evaluation of contact angle, $\theta$, of test liquids on polymer surfaces is used to determine the surface tension of these polymers.[1,2] In principle, a given pure liquid on an ideal (flat, homogeneous, smooth, rigid, and isotropic) solid should give a unique value for the equilibrium contact angle, $\theta_e$, as determined by Young's equation. However, in practice, a whole range of angles between advancing and receding values exists depending on the previous history of the triple line. The contact angle variability (or wetting hysteresis) is attributed to surface roughness and chemical heterogeneity.[3,4] On the other hand, the effect of the evaporation rate of the drop liquid is not so clear. The occurrence of liquid evaporation is inevitable unless the atmosphere in the immediate vicinity of the drop is saturated with the vapor of the liquid. A more complete understanding of how evaporation influences the contact angle of the drop on polymer surfaces in still air or in controlled atmospheric conditions is very important in the wetting and surface characterization processes.

There have been few studies concerning the rate of evaporation of a sessile drop on solid surfaces. Whitaker[5] reported the evaporation of water drops on a soot-covered surface, and the results showed that the surface area of the drop decreased with time. Morse[6] measured the evaporation of an iodine drop resting on a surface and determined that the rate of evaporation was proportional to the radius of the sphere. Langmuir[7] analyzed the results of Morse[6] and pointed out that the evaporation rate was reduced by the presence of the solid surface. Fuchs[8] stated that the evaporation rate could in some cases be proportional to the radius of curvature of the liquid−air interface. Picknett and Bexon[9] reported on the mass and profile evolution of methyl acetoacetate drops on poly(tetrafluoroethylene) (PTFE) surface in still air. They distinguished two modes of evaporation: at constant contact angle with diminishing contact area and at constant contact area with diminishing contact angle. They also observed a mixed type where the mode would change from one to the other at some point in the course of evaporation. In this mixed mode the drop shape would vary suddenly resulting in an increase in the contact angle with a decrease in the contact circle diameter or, sometimes, a decrease in both quantities. They developed a theory to predict the evaporation rate and residual mass at any time in the life of the drop based on the spherical cap geometry. However, the applicability of this theory was limited to drops smaller than 40 mg in weight due to the distortion of the shape of larger drops by gravity.[9]

Recently, Birdi et al.[10,11] reported the mass and contact diameter of water and *n*-octane drops placed on glass and PTFE. They observed that the rate of evaporation was dependent on the radius of the liquid−solid interface, $r_b$, by assuming a spherical cap geometry.[10] A model based on the diffusion of vapor across the boundary of a spherical cap drop was considered to explain their data. Later, this analysis was extended to determine the surface properties of porous solids.[12]

Shanahan et al.[13,14] examined the influence of evaporation on contact angles on polymer surfaces. They used water and *n*-decane drops on polyethylene, epoxy resin, and PTFE, both in saturated vapor atmosphere and in open air. The contact angle, $\theta$, and drop dimensions were measured as a function of time. A model was proposed to calculate the diffusion coefficient of the liquid vapor in air. Spherical cap geometry is used in all of their calculations, and it is concluded that a sessile drop deposited on a solid substrate may result only in an advancing value of the contact angle for a brief period of time if the local atmosphere is not saturated in the vapor of the liquid. The reason for this is that the evaporation of liquid from the drop meniscus will lower the contact angle. They have shown the existence of three stages in the evaporation process in open-air conditions: In the first stage, the contact radius, $r_b$, remains constant while $\theta$ and the drop height, $h$, decrease. In the second stage, $h$ and $r_b$ diminish concomitantly, thus maintaining $\theta$ more or less constant for smooth surfaces. This stage does not exist on rough surfaces.[14] In the final stage, the drop disappears in an irregular fashion with $h$, $r_b$, and $\theta$ tending

* Corresponding author, Fax 90 (262) 641 2309, e-mail hyerbil@mam.gov.tr.

† Also with TUBITAK, Marmara Research Center, Department of Mathematics, P.O. Box 21, 41470, Gebze, Kocaeli, Turkey.

⊗ Abstract published in *Advance ACS Abstracts,* June 1, 1997.

S1089-5647(97)00328-3 CCC: $14.00 

to zero. This step is difficult to follow experimentally, and it is probably related to the triple-line anchoring on local heterogeneous zones.[13] They have also showed that when the surrounding atmosphere is saturated in the vapor of the given liquid, the contact angle remains constant.[14] Kamusewitz et al.[15] and Yekta-Fard et al.[16] measured contact angles of drops in different atmospheres and showed $\theta$ to vary with the surrounding phase.

More recently, Rowan et al.[17] examined the change in the profile of small water droplets on poly(methyl methacrylate) (PMMA) due to evaporation in open air. Measurements of $\theta$ and the drop height, $h$, with time in the regime of constant contact radius, $r_b$, valid for $\theta < 90°$ were reported. It was proposed that the rate of mass loss which was calculated from the drop profile by assuming spherical cap geometry was proportional to $h$ and $r_b$ but not to the spherical radius, $R$. The results were explained by a model based on a two-parameter spherical cap geometry and the observed constant value of the contact radius. Rowan et al. examined only the first stage of drop evaporation where $r_b$ was constant, with $\theta$ and $h$ decreasing with time. They observed a critical angle which occurred at around 35−40° for water on PMMA, after which $r_b$ starts to contract.

In all the above evaporation studies the spherical cap geometry was used. It was assumed that when a drop of fluid is sufficiently small, the influence of gravity becomes negligible and the fluid forms a spherical cap shape.[18] Picknett and Bexon have reported that a drop resting on a smooth homogeneous surface takes the shape of a spherical cap provided that its mass is less than about 1 mg, and the drops larger than this mass are appreciably distorted by gravity.[9] The sessile drops are flattened, and oblate ellipsoid shapes are obtained when gravity effect is present. There is no theoretical analysis of evaporation from such drops.[9] However, information is available on the evaporation of prolate and oblate ellipsoids of revolution,[8] shapes which are similar to pendant and sessile drops with moderate gravity distortion and 90° contact angle, provided that only half the ellipsoid is considered. Padday has suggested that to have a shape similar to this oblate hemiellipsoid, a sessile drop of organic liquid must have a mass of about 40 mg.[19] The evaporation rate of a hemiellipsoid (either prolate or oblate) with the high axial ratio of 1.5 is calculated only about 2% faster than that for a hemisphere of the same volume, a difference which is assumed to be almost negligible in comparison with typical errors of measurement.[8]

There has been a debate in the literature whether the contact angle of a liquid on a solid is affected by drop size or gravity. Some researchers have taken into account the effect of gravity in experiments; for example, small drops have been used,[20,21] or $\theta$ has been measured under zero-gravity conditions, such as in free fall.[22] Pethica et al.[23] Leja and Poling[24] have proposed a model and explained theoretically that the contact angle is affected by gravity. Wada and Fukumoto[25] also calculated the effect of gravity on $\theta$ quantitatively using a spherical cap model. In contrast, some researchers suggested that the change in the contact angle with drop size was produced by hysteresis[26] or line tension effects[27] rather than the effect of gravity. Collins and Cooke[28] have shown that the 1957 paper by Pethica[23] to be false and have proved that gravity does not modify the contact angle. More recently, Fujii and Nakae[29] proposed a method showing the gravity had no effect on the equilibrium contact angle. However, although no gravity effect is present, shape distortion of liquid drops often occurs when the drop is placed on solid surfaces.

Since many distortions in liquid drops of very small drop volumes were detected in our previous studies,[30−32] we have decided to apply an ellipsoidal cap geometry in order to compare the differences between surface area, drop volume, and evaporation rates between the spherical and ellipsoidal cap geometry approaches. In this paper, Rowan et al.'s[17] precise $\theta$, $r_b$, and $h$ data of small water droplets on PMMA polymer is used for the calculations. An elliptical profile in the $x-y$ plane is revolved around the $y$-axis to form an ellipsoidal cap geometry for the drop, and the corresponding surface area and the volume of this body of revolution are found in terms of $r_b$, $h$, and $\theta$.

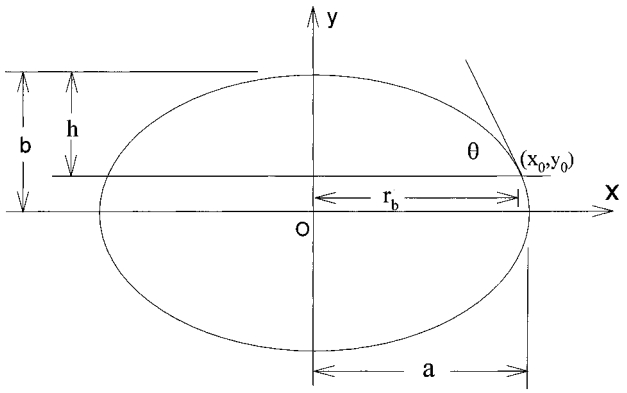


**Figure 1.** Geometry of an ellipsoidal cap-shaped drop on a solid.

## Theory

**Spherical Cap Model.** The spherical cap model is a two-parameter model. To evaluate the area and the volume of the spherical cap only two measured quantities, $r_b$ and $\theta$, or $h$ and $\theta$, or $r_b$ and $h$, may be used. When the parameters $r_b$ and $\theta$ are used, the surface area, $A$, of the liquid−air interface for a sessile drop is known to be

$$A = \frac{2\pi r_b^2}{1 + \cos\theta} \tag{1}$$

where $r_b$ is the contact radius between the solid−liquid interface, and $\theta$ is the contact angle. The volume of the drop is, on the other hand, given as

$$V = \frac{\pi r_b^3 (2 - 3\cos\theta + \cos^3\theta)}{3\sin^3\theta} \tag{2}$$

and the height of the spherical cap can be calculated from

$$h = r_b \tan(\theta/2) \tag{3}$$

**Three-Parameter Ellipsoidal Cap Model.** The ellipsoidal cap geometry, depicted in Figure 1, is a three-parameter model. It may be defined in terms of $r_b$, $h$, and $\theta$. All three measured quantities are required to evaluate the area and the volume of the ellipsoidal cap. The profile of the adopted liquid drop geometry in the $x-y$ plane is an ellipse with the equation

$$\frac{x^2}{a^2} + \frac{y^2}{b^2} = 1 \tag{4}$$

where $a$ and $b$ are the semiaxis lengths in the $x$ and $y$ directions, respectively. The point on the ellipse with the coordinates ($x_0$, $y_0$) in Figure 1 represents the physical triple point of the liquid drop, where $x_0 = r_b$ and $y_0 = b - h$.

It is found that the expressions can be summarized for all $\theta$ as follows:

$$a = \frac{r_b(s-h)}{\sqrt{s(s-2h)}} \quad (5)$$

$$b = \frac{h(s-h)}{s-2h} \quad (6)$$

$$y_0 = \frac{h^2}{s-2h} \quad (7)$$

where $s \equiv r_b \tan\theta$, and for $\theta = 90°$ a limit process is performed.

*Volume evaluation* (all cases of $\theta$): The volume of the ellipsoidal cap can be evaluated by rotating the curve about the $y$-axis for $y_0 \le y \le b$ resulting in

$$V = \pi\int_{y_0}^{b} x^2\,dy = \pi\frac{a^2}{b^2}\int_{y_0}^{b}(b^2 - y^2)\,dy \quad (8)$$

After integration one obtains

$$V = \frac{\pi a^2}{3b^2}(2b^3 - 3b^2y_0 + {y_0}^3) \quad (9)$$

By rearrangement using eqs 5−7, one obtains

$$V = \frac{\pi r_b}{3}\frac{h(2r_b\tan\theta - h)}{\tan\theta} \quad (10)$$

If $\theta = 90°$, then

$$V = \frac{2}{3}\pi {r_b}^2 h \quad (11)$$

*Surface area evaluation* (all cases of $\theta$): The surface area of the ellipsoidal cap can be calculated by rotating the curve about the $y$-axis for $y_0 \le y \le b$, resulting in

$$A = 2\pi\int_{y_0}^{b} x\sqrt{1 + (dx/dy)^2}\,dy \quad (12)$$

By differentiating eq 4 and combining it with eq 12, one obtains

$$A = (2\pi a/b^2)\int_{y_0}^{b}\sqrt{b^4 + (a^2 - b^2)y^2}\,dy \quad (13)$$

There may be three cases:

(1) If $a > b$, an oblate ellipsoidal cap is formed (as for sessile drop cases): By defining the eccentricity $e$ of an ellipse as

$$e \equiv \frac{\sqrt{a^2 - b^2}}{a} = \sqrt{1 - \left(\frac{b}{a}\right)^2} \quad (14)$$

the integration of eq 13 results in

$$A = \frac{\pi}{b^2 e}\{b^2[ea^2 + b^2\ln(eab + ab)] - y_0 ea\sqrt{(eay_0)^2 + b^4} - b^4\ln(y_0 ea + \sqrt{(eay_0)^2 + b^4})\} \quad (15)$$

(2) If $a < b$, a prolate ellipsoidal cap is formed (as for pendant drop cases): In this case, we define the eccentricity as follows:

$$e \equiv \frac{\sqrt{b^2 - a^2}}{b} = \sqrt{1 - \left(\frac{a}{b}\right)^2} \quad (16)$$

Hence, eq 13 leads to

$$A = \frac{\pi(1-e^2)}{ea}\left\{b^2[ea + b\sin^{-1}e] - y_0 e\sqrt{b^4 - eby_0^2} - b^3\sin^{-1}\left(\frac{ey_0}{b}\right)\right\} \quad (17)$$

(3) If $a = b$, then $e = 0$ and a spherical cap is formed with the surface area as given by eq 1.

*Vapor diffusion model:* Similar to Rowan et al.,[17] we assume that the evaporation rate is given by

$$\frac{dV}{dt} = -\frac{D}{\rho}\int\vec{\nabla}c\,d\vec{A} = -\frac{D}{\rho}\int\frac{\partial c}{\partial n}\,dA \quad (18)$$

where $D$ is the diffusion coefficient of the water vapor; $c$ is its concentration; $\rho$ is the density of the water; and the integral of the concentration gradient is taken over the surface of the ellipsoidal cap. To perform the integration in eq 18, the concentration gradient is assumed to be *radially* outward, and by distinguishing between the two radii of curvature, we assumed

$$\frac{\partial c}{\partial n} = \frac{(c_\infty - c_0)}{2}\left(\frac{1}{R_1} + \frac{1}{R_2}\right) \quad (19)$$

The radii of curvature $R_1$ and $R_2$ are given for a body of revolution as

$$\frac{1}{R_1} = \frac{-y''}{(1 + y'^2)^{3/2}} \quad (20)$$

$$\frac{1}{R_2} = \frac{-y'}{x(1 + y'^2)^{1/2}} \quad (21)$$

After rearrangement, eqs 20 and 21 become

$$\frac{1}{R_1} = \frac{ab^4}{[b^4 + (a^2 - b^2)y^2]^{3/2}} \quad (22)$$

$$\frac{1}{R_2} = \frac{b^2}{a[b^4 + (a^2 - b^2)y^2]^{1/2}} \quad (23)$$

Note that if $a = b$, then $e = 0$ and $R_1 = R_2 = a$ is obtained from eqs 22 and 23, thus reducing to the spherical cap geometry.

On the other hand, for the ellipsoidal cap

$$dA = \frac{2\pi a}{b^2}[b^4 + (a^2 - b^2)y^2]^{1/2}\,dy \quad (24)$$

is obtained from the differential area analysis, and it is now possible to perform the integration of eq 18. The evaporation rate is given as

$$\frac{dV}{dt} = -\frac{D\pi a(c_\infty - c_0)}{\rho}\left[\frac{1}{a}\int_{y_0}^{b}dy + ab^2\int_{y_0}^{b}\frac{dy}{b^4 + (a^2 - b^2)y^2}\right] \quad (25)$$

Similar to Rowan et al.[17] the various constants may be combined into a single factor:

$$\lambda = 2D\pi(c_\infty - c_0)/\rho \quad (26)$$

By performing the integrals in eq 25 for the case $a > b$, the evaporation rate expression is given as

$$\frac{dV}{dt} = -\lambda h\left[\frac{1}{2} + \frac{a}{2he}\left(\tan^{-1}\frac{ea}{b} - \tan^{-1}\frac{y_0 ea}{b^2}\right)\right] \quad (27)$$

where $h \equiv b - y_0$ by definition.

The limit of the second term in the above equation for $e \rightarrow 0$ gives

$$\lim_{e\rightarrow 0}\frac{a}{2he}\left(\tan^{-1}\frac{ea}{b} - \tan^{-1}\frac{y_0 ea}{b^2}\right) = \frac{1}{2} \quad (28)$$

Thus, eq 27 reduces to Rowan et al.'s spherical cap expression as $e \rightarrow 0$:

$$dV/dt = -\lambda h \quad (29)$$

**Two-Parameter Ellipsoidal Cap Model.** To proceed with eq 27 and derive a relationship between the contact angle and time, it has been found necessary to reduce the degrees of freedom in our model. In other words, instead of the three-parameter ellipsoidal model we propose at this point a two-parameter ellipsoidal model by using the initial experimental profile data to find the eccentricity of the ellipse. This eccentricity value is held constant for all times. As such, for $a > b$ and $1 > e \geq 0$, it can be found from eqs 5, 6, and 14 that

$$e^2 = 1 - \frac{h^2 \tan\theta}{r_b(r_b \tan\theta - 2h)} \quad (30)$$

and by defining

$$\alpha \equiv 1 - e^2 \quad (31)$$

The above equations can be solved for $h$ resulting in

$$h = r_b\frac{-\alpha + \sqrt{\alpha(\alpha + \tan^2\theta)}}{\tan\theta} \quad (32)$$

This equation also leads to

$$\tan\theta = \frac{2\alpha r_b h}{\alpha r_b^2 - h^2} \quad (33)$$

By combining eqs 10 and 33, one obtains for the volume of two-parameter ellipsoidal model the following expression:

$$V = \frac{\pi}{6\alpha}(3\alpha r_b^2 + h^2)h \quad (34)$$

*Vapor diffusion model*: To derive a simple vapor diffusion model consistent with the two-parameter ellipsoidal cap approach, the inverse tangent functions in eq 27 are taken equal to their arguments for small arguments values, i.e.

$$\tan^{-1}\frac{ea}{b} \cong \frac{ea}{b} \qquad \tan^{-1}\frac{y_0 ea}{b^2} \cong \frac{y_0 ea}{b^2} \quad (35)$$

Equation 27 is then simplified as

$$\frac{dV}{dt} \cong -\frac{(1+\alpha)}{2\alpha}\lambda h \quad (36)$$

If $V$ is defined as $V \equiv F(r_b,\alpha,h)$, then one obtains by the chain rule

$$\frac{dV}{dt} = \frac{\partial V}{\partial r_b}\frac{dr_b}{dt} + \frac{\partial V}{\partial \alpha}\frac{d\alpha}{dt} + \frac{\partial V}{\partial h}\frac{dh}{dt} \quad (37)$$

Since the eccentricity, $e$, can be calculated from the initial elliptical profile and may be assumed constant throughout the evaporation, one may hold $\alpha$, $r_b$ = constant, and eq 37 becomes

$$\frac{dV}{dt} = \frac{\partial V}{\partial h}\frac{dh}{dt} \quad (38)$$

By differentiating eq 34, one obtains

$$\frac{dV}{dh} = \frac{\pi}{2\alpha}(\alpha r_b^2 + h^2) \quad (39)$$

By combining eqs 36, 38, and 39, one obtains

$$-\frac{2\lambda}{\pi r_b^2}dt = \frac{2\alpha}{(1+\alpha)}\left[\frac{1}{h} + \frac{1}{\alpha r_b^2}h\right]dh \quad (40)$$

By integrating eq 40, one obtains

$$\varphi(h;\alpha) \equiv \frac{2\alpha}{(1+\alpha)}\left(\ln h + \frac{h^2}{2\alpha r_b^2}\right) = -\frac{2\lambda(t-c)}{\pi r_b^2} \quad (41)$$

where $\varphi = \varphi(\theta;r_b,\alpha)$ implicitly. Since

$$h = h(\theta) = \frac{r_b}{\tan\theta}[\sqrt{\alpha(\alpha + \tan^2\theta)} - \alpha] \quad (42)$$

one then obtains

$$F(\theta;\alpha) = \varphi[h(\theta);\alpha] = -\frac{2\lambda(t-c)}{\pi r_b^2} \quad (43)$$

where $F = F(\theta,r_b,\alpha)$ implicitly. To derive the left side of eq 43, eqs 41 and 42 are combined:

$$F(\theta;\alpha) = \frac{2\alpha}{(1+\alpha)}\left[\ln\frac{\sqrt{\alpha(\alpha+\tan^2\theta)} - \alpha}{\tan\theta} + \frac{\alpha + \tan^2\theta - \sqrt{\alpha(\alpha+\tan^2\theta)}}{\tan^2\theta}\right] = -\frac{2\lambda(t-c)}{\pi r_b^2} \quad (44)$$

It is noted that when $e = 0$, i.e., $\alpha = 1$, $F(\theta;\alpha)$ reduces to the $F(\theta)$ expression of Rowan.[17]

*For $a < b$:* The relevant equations can be obtained by substuting $\alpha^{-1}$ instead of $\alpha$ in eqs 32−44. The $F(\theta;\alpha)$ expression becomes

$$F(\theta;\alpha) = \frac{2\alpha}{(1+\alpha)}\left[\ln\frac{\sqrt{1+\alpha\tan^2\theta} - 1}{\alpha\tan\theta} + \frac{1 + \alpha\tan^2\theta - \sqrt{1+\alpha\tan^2\theta}}{\alpha\tan^2\theta}\right] = -\frac{2\lambda(t-c)}{\pi r_b^2} \quad (45)$$

## Results and Discussion

The recently published precise data of Rowan, Newton, and McHale[17] is used in the calculations. They applied water drops on poly(methyl methacrylate) (PMMA) as this gave a static contact radius and an initially large contact angle of around 80° which progressively decreased over a period of a few minutes. The temperature for all experiments was held constant within 0.5 °C at 21.5 °C, and the relative humidity was typically 55%. The contact radii were 0.293, 0.324, 0.381, 0.451, 0.491, and 0.585 mm and the approximate angular range was around 86−40°. The time dependence of the height is extracted directly from Figure 3 of ref 17, and that corresponding to the contact

**TABLE 1. Decrease of the Contact Angle, $\theta$, and Height, $h$, of Sessile Water Drops Having Different Initial Base Radius, $r_b$, on Poly(methyl methacrylate) Polymer Due to Evaporation in Air[17]**

| | $r_b = 0.585$ | | $r_b = 0.491$ | | $r_b = 0.451$ | | $r_b = 0.381$ | | $r_b = 0.324$ | | $r_b = 0.293$ | |
|---|---|---|---|---|---|---|---|---|---|---|---|---|
| time (min) | $\theta$ (deg) | $h$ (mm) | $\theta$ (deg) | $h$ (mm) | $\theta$ (deg) | $h$ (mm) | $\theta$ (deg) | $h$ (mm) | $\theta$ (deg) | $h$ (mm) | $\theta$ (deg) | h (mm) |
| 0.25 | | | | | | | | | 81.3 | 0.261 | 86.0 | 0.248 |
| 0.50 | 78.9 | 0.486 | 80.7 | 0.394 | 75.6 | 0.343 | 79.4 | 0.301 | 78.0 | 0.253 | 81.6 | 0.238 |
| 0.75 | | | | | | | | | 75.4 | 0.236 | 80.8 | 0.230 |
| 1.00 | 76.8 | 0.469 | 79.4 | 0.390 | 72.0 | 0.322 | 75.9 | 0.292 | 72.4 | 0.229 | 76.6 | 0.217 |
| 1.25 | | | | | | | | | 70.8 | 0.214 | 74.0 | 0.209 |
| 1.50 | 75.0 | 0.461 | 76.8 | 0.382 | 70.7 | 0.316 | 71.3 | 0.276 | 66.9 | 0.205 | 73.0 | 0.197 |
| 1.75 | | | | | | | | | 65.8 | 0.200 | 67.8 | 0.184 |
| 2.00 | 75.2 | 0.447 | 73.7 | 0.364 | 67.2 | 0.300 | 68.8 | 0.258 | 62.6 | 0.186 | 65.1 | 0.170 |
| 2.25 | | | | | | | | | 60.1 | 0.169 | 61.4 | 0.163 |
| 2.50 | 71.6 | 0.436 | 72.4 | 0.354 | 64.0 | 0.284 | 63.7 | 0.239 | 56.4 | 0.158 | 57.8 | 0.146 |
| 2.75 | | | | | | | | | 52.0 | 0.150 | 56.7 | 0.139 |
| 3.00 | 71.8 | 0.419 | 70.3 | 0.337 | 62.1 | 0.268 | 59.9 | 0.220 | 51.7 | 0.144 | 53.5 | 0.129 |
| 3.25 | | | | | | | | | 47.0 | 0.126 | | |
| 3.50 | 69.3 | 0.408 | 67.8 | 0.321 | 58.3 | 0.252 | 57.6 | 0.202 | | | | |
| 4.00 | 68.6 | 0.397 | 64.4 | 0.304 | 54.3 | 0.236 | 50.0 | 0.182 | | | | |
| 4.50 | 66.6 | 0.384 | 61.4 | 0.288 | 49.8 | 0.220 | 45.5 | 0.169 | | | | |
| 5.00 | 64.0 | 0.370 | 57.7 | 0.274 | 46.9 | 0.204 | | | | | | |
| 5.50 | 63.1 | 0.358 | 55.0 | 0.253 | 44.0 | 0.193 | | | | | | |
| 6.00 | 61.4 | 0.344 | 53.0 | 0.238 | 39.4 | 0.177 | | | | | | |
| 6.50 | 59.0 | 0.326 | | | | | | | | | | |

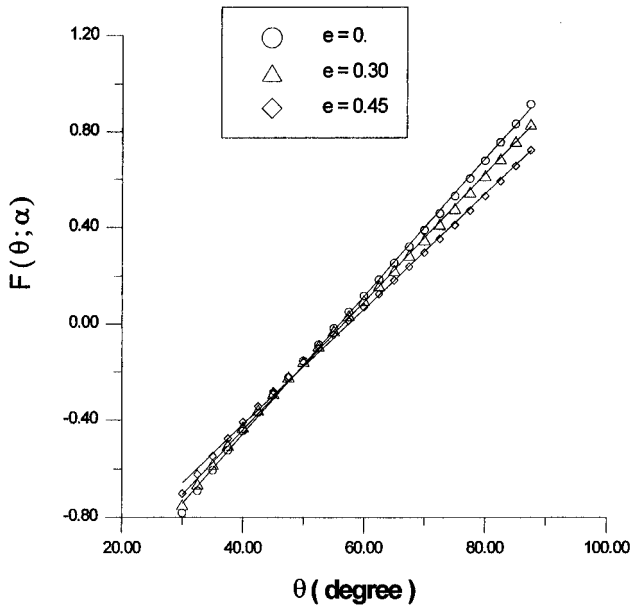


**Figure 2.** Plot of the angular function $F(\theta;\alpha)$ in the two-parameter ellipsoidal model against consecutive contact angles for $e = 0$ (○), $e = 0.30$ (△), $e = 0.45$ (◇).

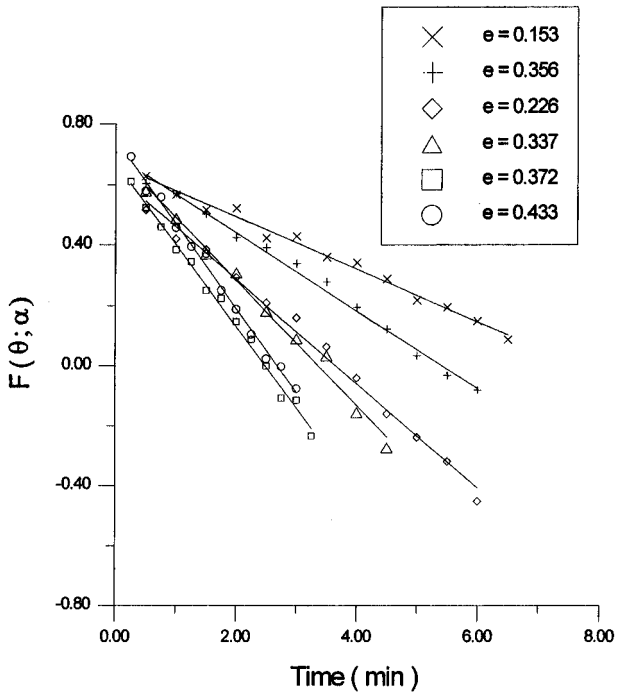


**Figure 3.** Time dependencies of the two-parameter angular function $F(\theta;\alpha)$ for contact radii 0.293 (○), 0.324 (□), 0.381 (△), 0.451 (◇), 0.491 (+), and 0.585 mm (×) using the measured values of $\theta$.

angle from Figure 2 of the same reference through the angular function equation given as

$$F(\theta) = \ln[\tan(\theta/2)] + \frac{1 - \cos\theta}{\sin^2\theta} \qquad (46)$$

All the data are listed in Table 1. The angular function of the two-parameter ellipsoidal model $F(\theta;\alpha)$ (eq 44) for different eccentricity values is plotted against the contact angle in Figure 2. When $e = 0$, i.e., $\alpha = 1$, $F(\theta;\alpha)$ reduces to the $F(\theta)$ expression of Rowan, i.e., eq 46, and it is seen that an increase in the eccentricity decreases the slope of the straight-line fit over the range 86−30°. Over this range the fit is very good similar to Rowan's plot.

In Figure 3 we plot the function $F(\theta;\alpha)$, defined by eqs 44 and 45 against time for six different contact radii ranging from 0.293 to 0.585 mm using the measured values of contact angles ranging from around 86° to 40°. Each data set can be fitted to straight lines indicating the linear time dependence of the $F(\theta;\alpha)$ function.

In Figure 4 we plot the time behavior of the drop heights: as measured experimentally; as calculated from spherical cap geometry by using eq 3; and as calculated from the two-parameter ellipsoidal cap geometry using eqs 32. In this figure, a clear linearity of the experimental heights with time is recognized, and it is seen that the heights calculated from the ellipsoidal cap geometry fit the experimental heights better than the spherical cap geometry. The ellipsoidal model will necessarily fit the data at the initial point due to the definition of eccentricity; however, the fit is also very good for most of the total data.

In Figure 5 we plot the contact angles $\theta$ against time for the

**TABLE 2. Eccentricity, *e*, and Related α Values for the Initial Drop Profiles**

| $r_b$ (mm) | $\theta$ (deg) | $h$ (mm) | $a$ (mm) | $b$ (mm) | $a/b$ | $e$ | α |
|---|---|---|---|---|---|---|---|
| 0.585 | 78.9 | 0.486 | 0.596 | 0.603 | 0.99 | 0.153 | 0.977 |
| 0.491 | 80.7 | 0.394 | 0.497 | 0.464 | 1.07 | 0.356 | 0.873 |
| 0.451 | 75.6 | 0.343 | 0.465 | 0.453 | 1.03 | 0.226 | 0.949 |
| 0.381 | 79.4 | 0.301 | 0.387 | 0.364 | 1.06 | 0.337 | 0.886 |
| 0.324 | 81.3 | 0.261 | 0.327 | 0.304 | 1.08 | 0.372 | 0.861 |
| 0.293 | 86.0 | 0.248 | 0.294 | 0.265 | 1.11 | 0.433 | 0.813 |

**TABLE 3. Arithmetic Mean Values of Surface Area, *A*, and Volume, *V*, of Water Drops As Calculated with the Spherical and Ellipsoidal Cap Models for Different Contact Radii**

| contact radius, $r_b$ (mm) | spherical cap area, $A$ (mm$^2$) | ellipsoidal cap area, $A$ (mm$^2$) | spherical cap volume, $V$ (mm$^3$) | ellipsoidal cap volume, $V$ (mm$^3$) |
|---|---|---|---|---|
| 0.585 | 1.803 | 1.812 | 0.317 | 0.320 |
| 0.491 | 1.304 | 1.264 | 0.196 | 0.186 |
| 0.451 | 1.023 | 1.013 | 0.134 | 0.132 |
| 0.381 | 0.770 | 0.750 | 0.089 | 0.085 |
| 0.324 | 0.573 | 0.553 | 0.057 | 0.054 |
| 0.293 | 0.504 | 0.476 | 0.047 | 0.043 |

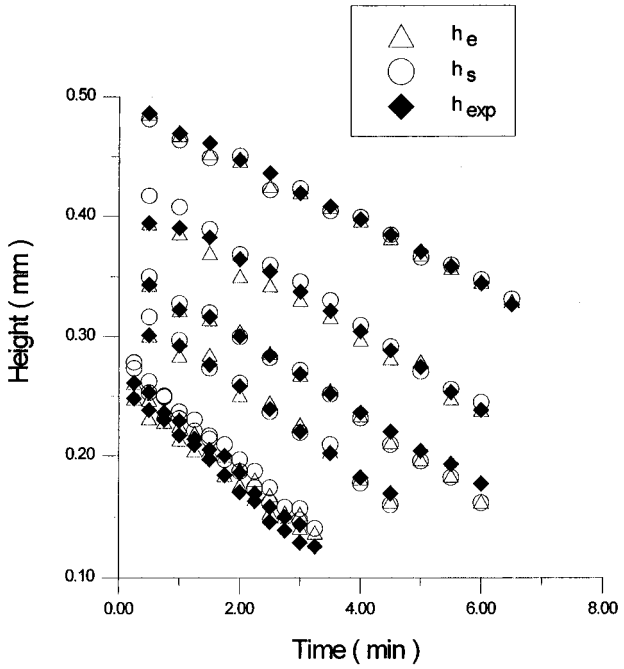


**Figure 4.** Time dependencies of water drop heights as calculated from the spherical cap geometry (○), from the two-parameter ellipsoidal cap geometry (△), and for the experimental data (◆) for all the drops.

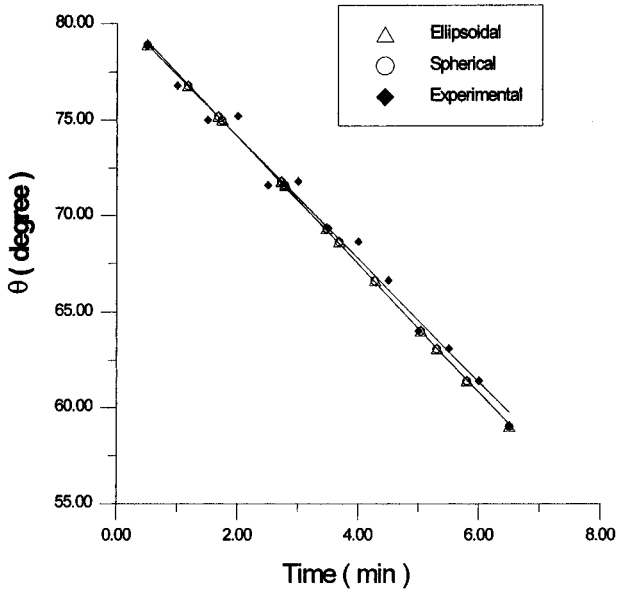


**Figure 5.** Time dependencies of the water contact angles as calculated from the spherical cap geometry (○), from the two-parameter ellipsoidal cap geometry (△), and for the experimental data (◆) for the single drop with $r_b = 0.585$ mm.

data set of the largest drop with $r_b = 0.585$ mm: as measured experimentally; as calculated from the ellipsoidal cap diffusion model using eq 44 or 45; and as calculated from the spherical cap geometry using the same equations with $e = 0$, i.e., $\alpha = 1$. The integration constant $c$ and the constant $\lambda$ in the above-mentioned equations are calculated from experimental initial and final data. In this figure, it is seen that the straight-line fits of the spherical and ellipsoidal cap (with $e = 0.153$) models are nearly coincidental with each and close the straight-line fit of the experimental data. The agreement of both models with the experiment is, in a way, to be expected knowing the time behavior of the angular function $F(\theta;\alpha)$ and also for the reason that the constants $c$ and $\lambda$ have been evaluated at two (initial and final) time points. A similar plot for the time dependency of the contact angle $\theta$ has provided for the smallest drop with $r_b = 0.293$ mm and $e = 0.433$ in Figure 6. Even for the large eccentricity for this drop, the agreement of the present results with experimental data is also very good in this figure.

The surface area $A$ of the water drops for the spherical cap model is calculated by using eq 1, and for the three-parameter ellipsoidal cap model by using eqs 5−7, 15, and 17, and their arithmetic mean values are given in Table 3. The volumes of water drops, $V$, for the spherical cap model are calculated by using eq 2, and for the three-parameter ellipsoidal cap model by using eqs 5−7 and 9 or 10, and their arithmetic mean values are given in Table 3. As seen from Table 3, the three-parameter ellipsoidal cap model gives smaller surface area values for all the drops than those of the spherical cap model except the largest drop. Also, the three-parameter ellipsoidal cap model gives smaller volume values for all the drops than those of the spherical cap model except the largest drop. It is possible that a small experimental error had occurred during the determination of the profile of the largest drop because its $a/b$ ratio was 0.99 as seen in Table 2, indicating that the shape was opposite of flattened (with a very small deviation from the spherical shape), whereas all the other drops had their $a/b$ ratios larger than 1 (between 1.03 and 1.11), indicating slightly flattened shapes. It should be noted that an assumption indicating that a drop having a slightly ellipsoidal (flattened) shape will end up spherical shape by evaporation seems physically reasonable, but this does not fit the experimental findings. When eq 3 is used to test the experimental height data by using experimental $r_b$ and $\theta$ values,

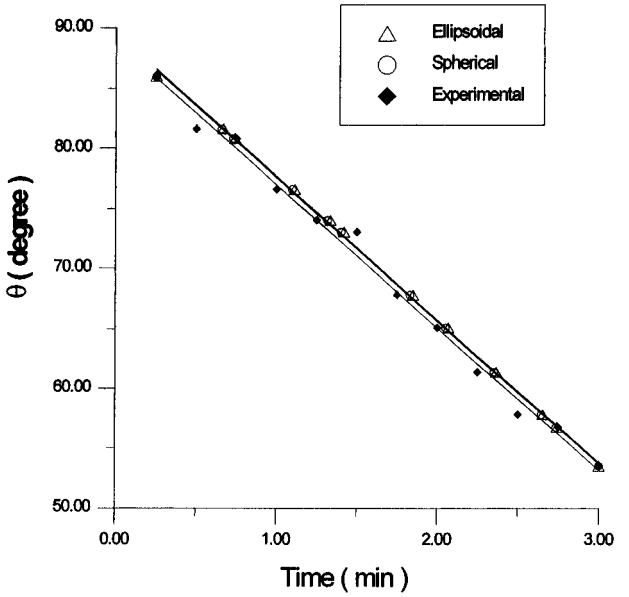


**Figure 6.** Time dependencies of the water contact angles as calculated from the spherical cap geometry (○), from the two-parameter ellipsoidal cap geometry (△), and for the experimental data (◆) for the single drop with $r_b = 0.293$ mm.

the deviations from the spherical cap shape sometimes get larger in an increasing order when the drop size decreases by evaporation. Due to this reason it is believed that the three-parameter ellipsoidal model expresses the area and volume of the evaporating drops better than the spherical cap model. When the three-parameter ellipsoidal model is applied, the surface area and the volume of the drops showed an almost complete linear time dependence for most of the data. To test all the models, experimental $V$ values are required that are lacking in Rowan et al. data.[17] A simultaneous experimental measuring of the weight, $\theta$, $h$, and $r_b$ of the drops may satisfy such a test in the future.

It should be pointed out that the Rowan et al.[17] used very small water droplets with $r_b = 0.293-0.585$ mm to exclude any gravity and other geometric distortion effects. In the usual contact angle practice, drops with $r_b = 0.5-1.5$ mm are generally used without any reservation of spherical cap geometry.[10,13,30−32] According to our analysis, the ellipsoidal cap geometry should be applied for such large drop cases in order to eliminate any distortion effects in contact angle evaluations.

## Conclusion

The rate of evaporation of small water droplets on PMMA has been analyzed by using the data provided by Rowan et al.[17]

Mathematical expressions for a three-parameter ellipsoidal cap model are derived for the drop shapes. When this ellipsoidal model is applied, the surface area, $A$, and the volume, $V$, of the drops showed an almost complete linear time dependence for most of the data. One may speculate that the distortions of spherical cap geometry begin in the 0.3−0.5 mm drop size range and the ellipsoidal cap geometry may be considered in the usual contact angle measurement sizes of $r_b = 0.5-1.5$ mm.

A vapor diffusion model depending on the two radii of curvature of the three-parameter ellipsoidal cap geometry is developed similar to Rowan et el.'s spherical cap model. The present rate of evaporation expression reduces to that of Rowan et al.'s in the limit as the drop shape becomes a spherical cap geometry.

To derive a relationship between the contact angle and time, the degrees of freedom in the three-parameter ellipsoidal model are reduced and a two-parameter ellipsoidal cap model is developed by assuming the eccentricity obtained from the initial experimental drop profile as constant for all times. When this analysis is applied, the heights as calculated from the two-parameter ellipsoidal cap model fit the experimental data better than the heights calculated from the spherical cap model.

An excellent agreement of the ellipsoidal (along with the spherical) model with the experimental data to predict the contact angle change with time has been presented.

This agreement is a valid proof for the success of both the spherical and ellipsoidal diffusion models.

**Acknowledgment.** The authors express their thanks to Dr. G. McHale of the Nottingham Trent University for supplying the correct experimental data of Figures 2 and 3 of ref 17. R.A.M. also appreciates the financial support provided by the Research Fund of the Istanbul Technical University.

## References and Notes

(1) Erbil, H. Y. *Langmuir* **1994**, *10*, 2006.
(2) Erbil, H. Y. Surface Tension of Polymers. In: *Handbook of Surface and Colloid Chemistry*; Birdi, K. S., Ed.; CRC Press Inc.: Boca Raton, FL, 1997; Chapter 9, in press.
(3) Johnson, R. E.; Dettre, R. H. *J. Phys. Chem.* **1964**, *68*, 1744.
(4) De Gennes, P. G. *Rev. Mod. Phys*. **1985**, *57*, 827.
(5) Whitaker, H., In: *Smoke*; Whytlaw-Gray, R., Patterson, H. S., Eds.; Arnold: London, 1932; p 172.
(6) Morse, H. W. *Proc. Am. Acad. Arts Sci*. **1910**, *45*, 363.
(7) Langmuir, I. *Phys. Rev*. **1918**, *12*, 368.
(8) Fuchs, N. A. *Evaporation and Droplet Growth in Gaseous Media*; Pergamon Press: London, 1959; p 6.
(9) Picknett, R. G.; Bexon, R. *J. Colloid Interface Sci*. **1977**, *61*, 336.
(10) Birdi, K. S.; Vu, D. T.; Winter, A. *J. Phys. Chem.* **1989**, *93*, 3702.
(11) Birdi, K. S.; Vu, D. T.; Andersen, S. I.; Winter, A.; Topsoe, H.; Christensen, S. V. In: *Characterization of Porous Solids II*; Elsevier: Amsterdam, 1991; p 151.
(12) Birdi, K. S.; Vu, D. T. *J. Adhesion Sci. Technol*. **1993**, *7*, 485.
(13) Shanahan, M. E. R. and Bourges, C. *Int. J. Adhesion Adhesives* **1994**, *14*, 201.
(14) Bourges-Monnier, C.; Shanahan, M. E. R. *Langmuir* **1995**, *11*, 2820.
(15) Kamusewitz, H.; Possart, W.; Paul, D. *Int. J. Adhesion Adhesives* **1993**, *13*, 243.
(16) Yekta-Fard, M.; Ponter, A. B. *J. Colloid Interface Sci.* **1988**, *126*, 134.
(17) Rowan, S. M.; Newton, M. I.; McHale, G. *J. Phys. Chem*. **1995**, *99*, 13268.
(18) Leger, L.; Joanny, J. F. *Rep. Prog. Phys*. **1992**, *55*, 431.
(19) Padday, J. F. *Philos. Trans. R. Soc. London A* **1971**, *269*, 265.
(20) Mehrotra, S. P.; Chaklader, A. C. D. *Metall. Trans*. **1985**, *16B*, 567.
(21) Yokota, M.; Fukuda, N., Nagai, H.; Shoji, K. *J. Jpn. Inst. Metall.* **1989**, *53*, 439.
(22) Shimizu, S.; Kusunose, T.; Kimura, H.; Ooyama, M.; Imura, M.; Ishikura, S.; Sahira, K.; Kitamura, H.; Shiraishi, H.; Nakada, Y.; Wada, M.; Suzuki, M.; Narita, T. Parabolic Flight, NASDA-JSUP, 1991; Vol. 1, p 49.
(23) Pethica, B. A.; Pethica, P. J. C. *Proc. 2nd. Int. Congr. Surface Activity (London)*; Butterworth: London, 1957; Vol. 3, p 131.
(24) Leja, J.; Poling, G. W. *Proc. Int. Mineral Process. Congr. Paper No. 17, Group III* **1960**, 325.
(25) Wada, T.; Fukumoto, T. *J. Jpn. Inst. Welding* **1968**, *37*, 845.
(26) Herzberg, W. J.; Marian, J. E. *J. Colloid Interface Sci.* **1970**, *33*, 161.
(27) Good, R. J.; Koo, M. N. *J. Colloid Interface Sci*. **1979**, *71*, 283.
(28) Collins, R. E.; Cooke, C. E. *Trans. Faraday Soc*. **1959**, *55*, 1602.
(29) Fujii, H.; Nakae, H. *Philos. Mag. A* **1995**, *72*, 1505.
(30) Erbil, H. Y. *J. Appl. Polym. Sci*. **1987**, *33*, 1397.
(31) Erbil, H. Y.; Hazer, B. *J. Appl. Polym. Sci.* **1996**, *60*, 1313.
(32) Erbil, H. Y. *Polymer* **1996**, *37*, 5483.